Supplementary Figure legend

Figure S1 Related to Figure 1 Recording sites. (**a**) MRI images. Electrode tracks to pulvinar are shown as the black, tracks to IT are shown as yellow arrows. Images for V4 shows the location of recording chambers. (**b**) Estimate of recording sites in pulvinar. The red lines represent the estimated spatial range of recordings. (**c**) Estimate of recording sites in IT. The red lines represent the estimated spatial range of recordings.

Figure S2 Related to Figure 2 Visual response properties of neurons in V4, IT and pulvinar. (**a**) Spatial tuning of neurons across three locations tested in the contralateral field. Location with strongest responses defined as the best location and location with weakest responses defined as the worst location. (**b**) Stimulus tuning of neurons across the 7 tested stimuli. (**c**) Cumulative distributions of visual response latencies in the three areas. (**d**) The population averages of V4, IT and pulvinar visual responses to their preferred object at the best location in their RFs. V4, n=310; pulvinar, n=339; IT, n=210.

Figure S3 Related to Figure 3 Spike–LFP coherence, firing rate and LFP power. (**a**) Spike–LFP coherence after equalizing firing rates and LFP power in Attention In and Attention Out conditions. Left: spike-LFP coherence after equalization; middle: LFP power; right: firing rates. The LFP power at gamma frequencies (30-60Hz) and firing rates in Attention In and Attention Out conditions are not significantly different (Wilcoxon rank sum test, $P > 0.05$). (**b**) Correlations between pulvinar spiking activity and V4 and IT LFP power at difference frequencies.

Figure S4 Related to Figure 4 Granger Causality in different directions, in pre-stimulus period and after LFP power equalization. (**a**) Comparisons of Granger causality between V4 and pulvinar (Pulv; n=1608). Left plot: a comparison of the Granger causalities in Attention In condition. The population averages of the Granger causality in the two directions are shown. The SEM (±) of the population average is marked by the shading above and below the averages. Right plot: a comparison of the Granger causalities in Attention Out condition. (**b**) Comparison of Granger causalities between V4 and IT (n=1072). (**c**) Comparison of Granger causalities between pulvinar and IT (n=1720). Formats in (**b**) and (**c**) is the same as the format in (**a**). (**d**) Granger causality between V4 and pulvinar (Pulv) during the last 256ms period prior to the onset of three object stimuli in the cue-first sessions (n=960). (**e**) Granger causality between V4 and pulvinar after LFP power equalization. The two left plots show granger causality after the power equalization. The two right plots show V4 and pulvinar LFP powers, respectively. LFP powers at gamma frequencies (30-60Hz) in Attention In and Attention Out conditions are not significantly different (Wilcoxon rank-sum test, $P > 0.05$). (**f**)) Granger causality between V4 and IT after LFP power equalization.

Figure S5 Related to Figure 5 Time shift of gamma oscillations between areas. (**a**) Left plot: distribution of time shifts between V4 and pulvinar gamma oscillations. The black bars show distribution of time shifts from LFP-LFP pairs whose gamma phase shifts increased or decreased linearly with frequency significantly (multiple linear regression, $P<0.05$). The blue bars show distribution from LFP-LFP pairs whose gamma phase shifts did not change linearly with frequency significantly (multiple linear regression, $P>0.05$). Right plot: the averaged absolute value of residual at different gamma frequencies from linear regression significant LFP-LFP pairs (black bars) and non-significant LFP-LFP pairs (Blue bars). At all gamma frequencies, the absolute value of residual

was significantly higher from linear regression non-significant LFP-LFP pairs than from linear regression significant LFP-LFP pairs (Wilcoxon rank sum test, $P < 0.05$). (**b**) Distribution of time shifts between V4 and IT gamma oscillations from linear regression significant and non-significant LFP-LFP pairs. (**c**) V4 recording sites and time shifts between V4 and pulvinar gamma oscillations. The V4 sites are divided into two groups based on recording channel number: upper 8 channels and low 8 channels. There are three different types of V4-pulvinar LFP pairs: V4 lead (V4 gamma leads pulvinar gamma), V4 lag (pulvinar gamma leads V4 gamma), and non-significant (linear regression non-significant LFP-LFP pairs) pairs.

Figure S6 Related to Figure 6 Visual stimuli, firing rate changes and performance during deactivation sessions. (**a**) During pulvinar deactivation sessions, the three stimuli in the spatial attention task were displayed in both hemifields. One stimulus was in the ipsilateral field to the recording side, and the other two were in the field contralateral to the recordings. (**b**) Performance in the spatial attention task without distracters. In this condition, only one target stimulus (without distracters) appeared in the spatial attention task. Muscimol injection in pulvinar selectively lowered monkeys' performance at the location corresponding to the RF of recorded V4 neurons, while performance at the other two locations outside of the V4 RF (Out-1 and Out-2) were not affected. The averaged performance across 8 sessions and the SEM (±) of the averaged performance are shown here. (**c**) – (**d**) Effects of pulvinar deactivation on attentional modulation (**c**) and visual response (**d**) in V4 recorded by deep 8 channels. (**e**) – (**f**) Effects of pulvinar deactivation on attentional modulation (**e**) and visual response (**f**) in V4 recorded by upper 8 channels. (**g**) – (**h**) Effects of pulvinar deactivation on visual response in LGN and V4 neurons in the same deactivation sessions. (**g**) Averaged visual response of LGN neurons before and after pulvinar deactivation. (**h**) Averaged visual response of V4 neurons before and after pulvinar deactivation. (**i**) Effects of pulvinar deactivation on IT population response.

Figure S7 Related to Figure 7 Effects of pulvinar deactivation on coherence, LFP power and current source density (CSD) in V4. (**a**)-(**b**) Effects on V4 spike–V4 LFP coherence in the deep 8 recording channels (a) and upper 8 channels (**b**). (**c**) Distributions of phase shifts between V4 and IT low frequency LFPs before and after the pulvinar deactivation. Left plot shows distributions in Attention In conditions; right plot shows distribution in Attention Out condition. (**d**) Effects of pulvinar deactivation on V4 CSD in Attention In and Attention Out conditions. (**e**)-(**f**) Effects on V4 LFP powers in the upper 8 recording channels (**e**) and the deep 8 channels (**f**).

Figure S8 Related to Figure 7 and 8 Effects of pulvinar deactivation on V4 and IT LFP power and coherence . (**a**) Effects on V4 LFP power in Baseline period. The Baseline period was the last 250ms period before the onset of the three object stimuli. Left plot shows population averages of V4 LFP power spectrum before and after muscimol injection in Attention In condition. Right plot shows the population averages in Attention Out condition. (**b**) Effects on IT LFP power in Baseline period. (**c**) Effects on IT LFP power in Delay period. The Delay period was the last 256 ms period before the color change in the spatial attention task. (**d**) Effects on V4 LFP power in a 2000 ms period from 1500 ms before to 500 ms after the color change. Formats in (**b**) - (**d**) are the same as the format in (**a**). (**e**) Effects on coherence between V4 LFPs from upper 8 channels and IT LFPs. (**f**) Effects on coherence between V4 LFPs from deep 8 channels and IT LFPs. (**g**) Effects of deactivation on V4 LFP power on short delay trials. The delays of the short trials were shorter than the mean delay length in a session. (**h**) Effects of deactivation on V4 LFP power on long delay trials. The delays of the long trials were longer than the mean delay length in a session.

Figure S1

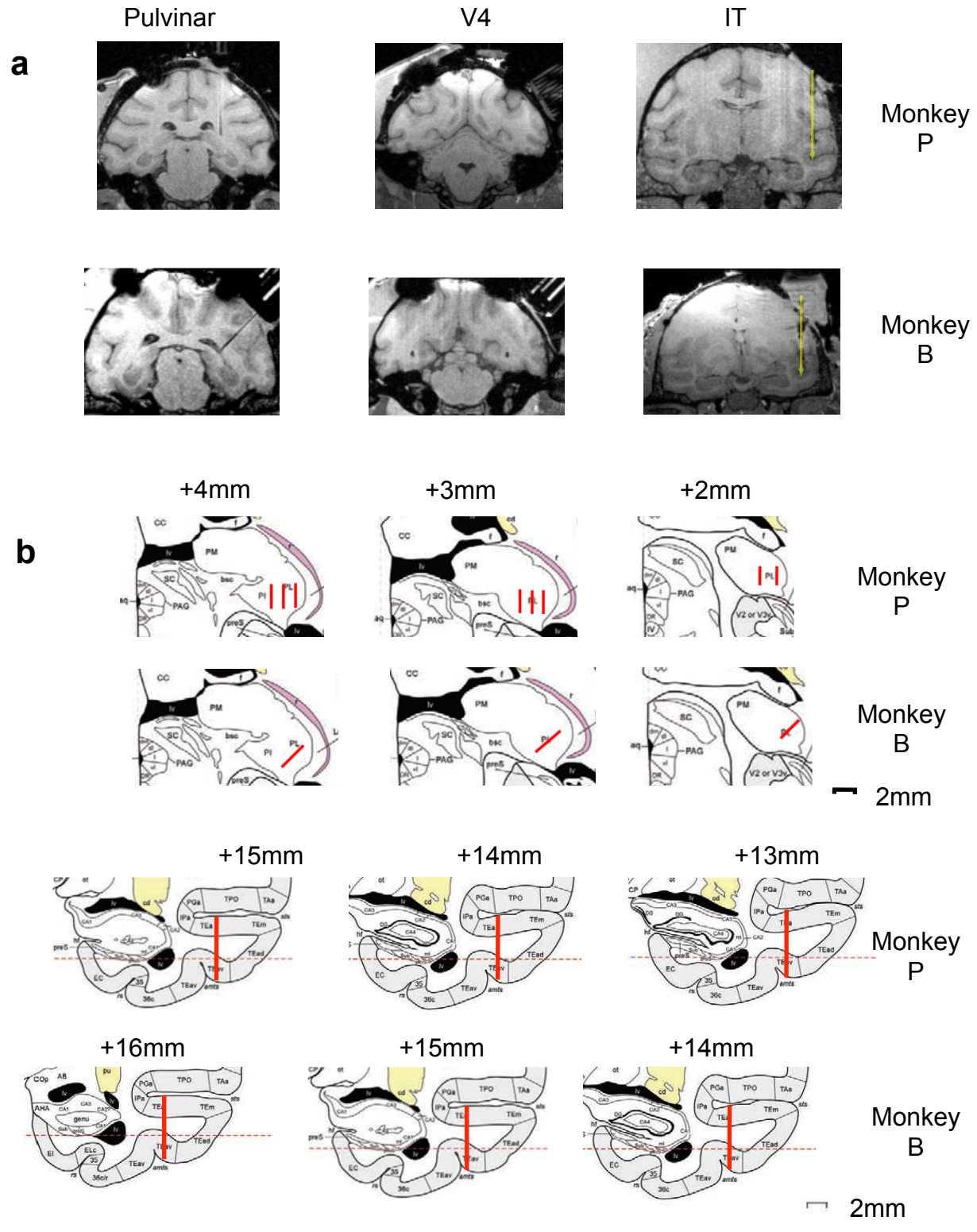
a
Pulvinar
V4
IT
Monkey P
Monkey B
b
+4mm
+3mm
+2mm
Monkey P
Monkey B
2mm
c
+15mm
+14mm
+13mm
Monkey P
+16mm
+15mm
+14mm
Monkey B
2mm

Figure S2

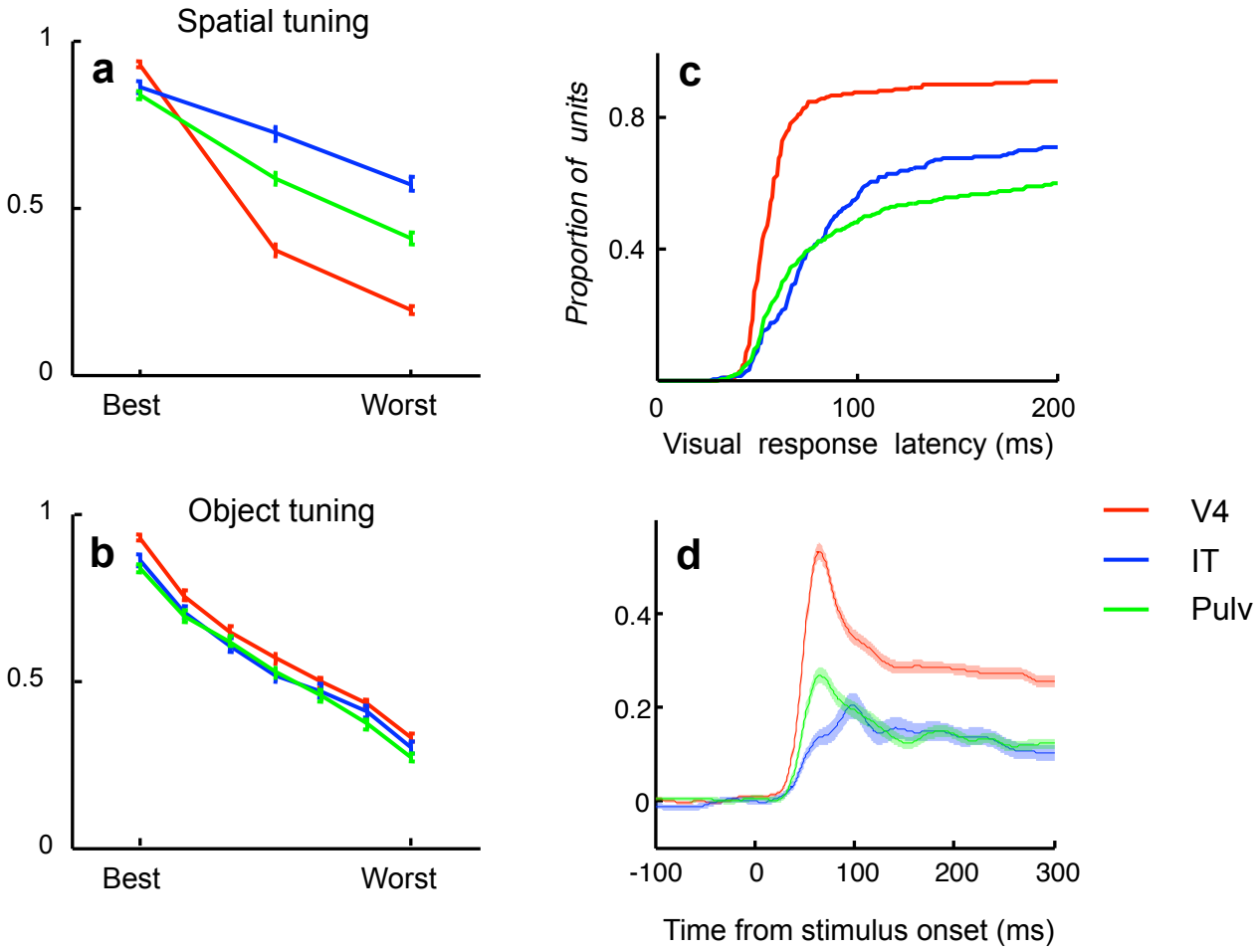
Spatial tuning
a
1
0.5
0
Best
Worst
Object tuning
b
1
0.5
0
Best
Worst
c
Proportion of units
0.8
0.4
0
100
200
Visual response latency (ms)
d
0.4
0.2
0
-100
0
100
200
300
Time from stimulus onset (ms)
V4
IT
Pulv

Figure S3

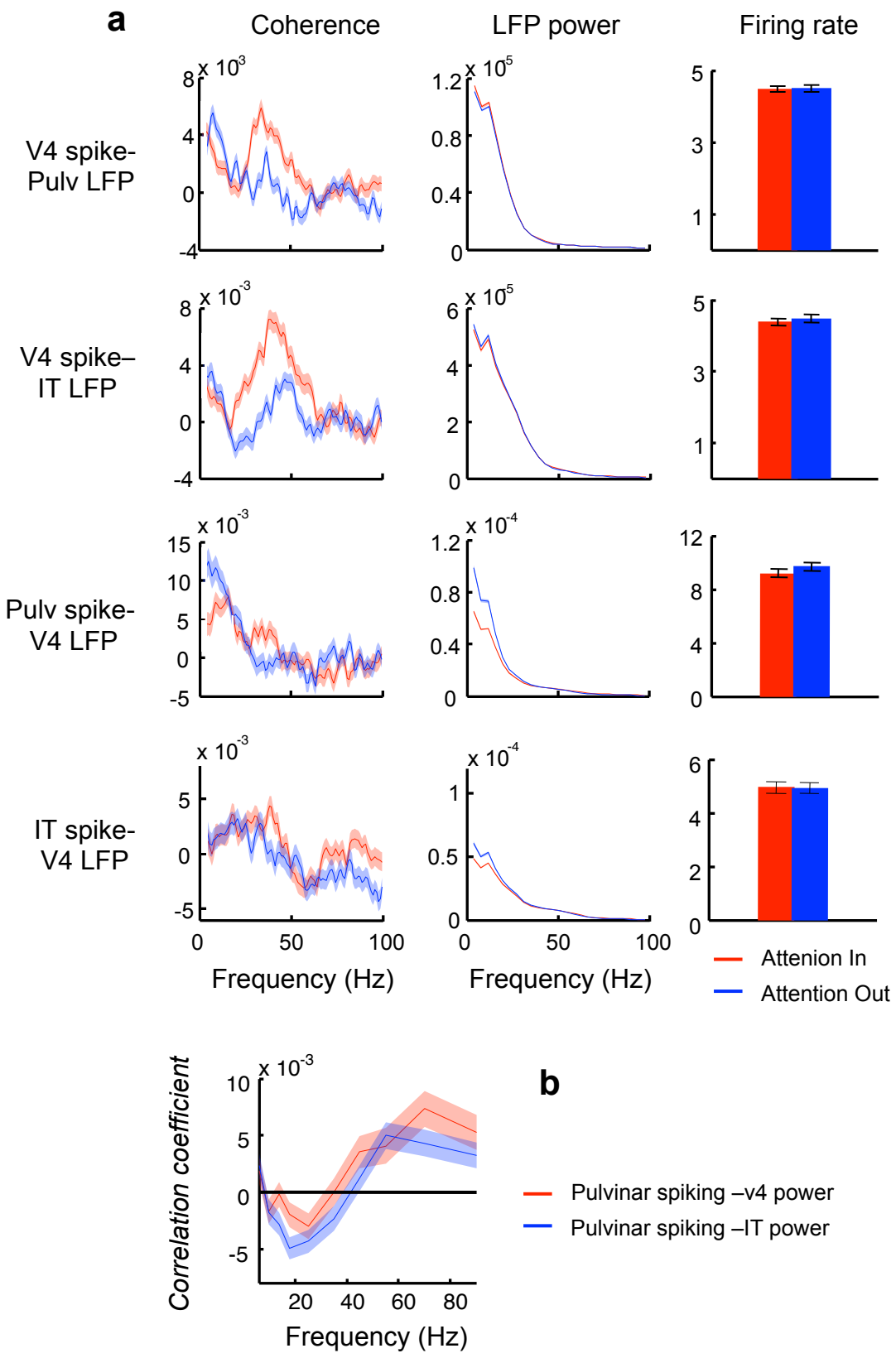
a
Coherence
LFP power
Firing rate
V4 spike-
Pulv LFP
V4 spike–
IT LFP
Pulv spike-
V4 LFP
IT spike-
V4 LFP
x 10^3
x 10^5
x 10^-3
x 10^5
x 10^-3
x 10^-4
x 10^-3
x 10^-4
Frequency (Hz)
Frequency (Hz)
Attenion In
Attention Out
b
Correlation coefficient
x 10^-3
Frequency (Hz)
Pulvinar spiking –v4 power
Pulvinar spiking –IT power

Figure S4

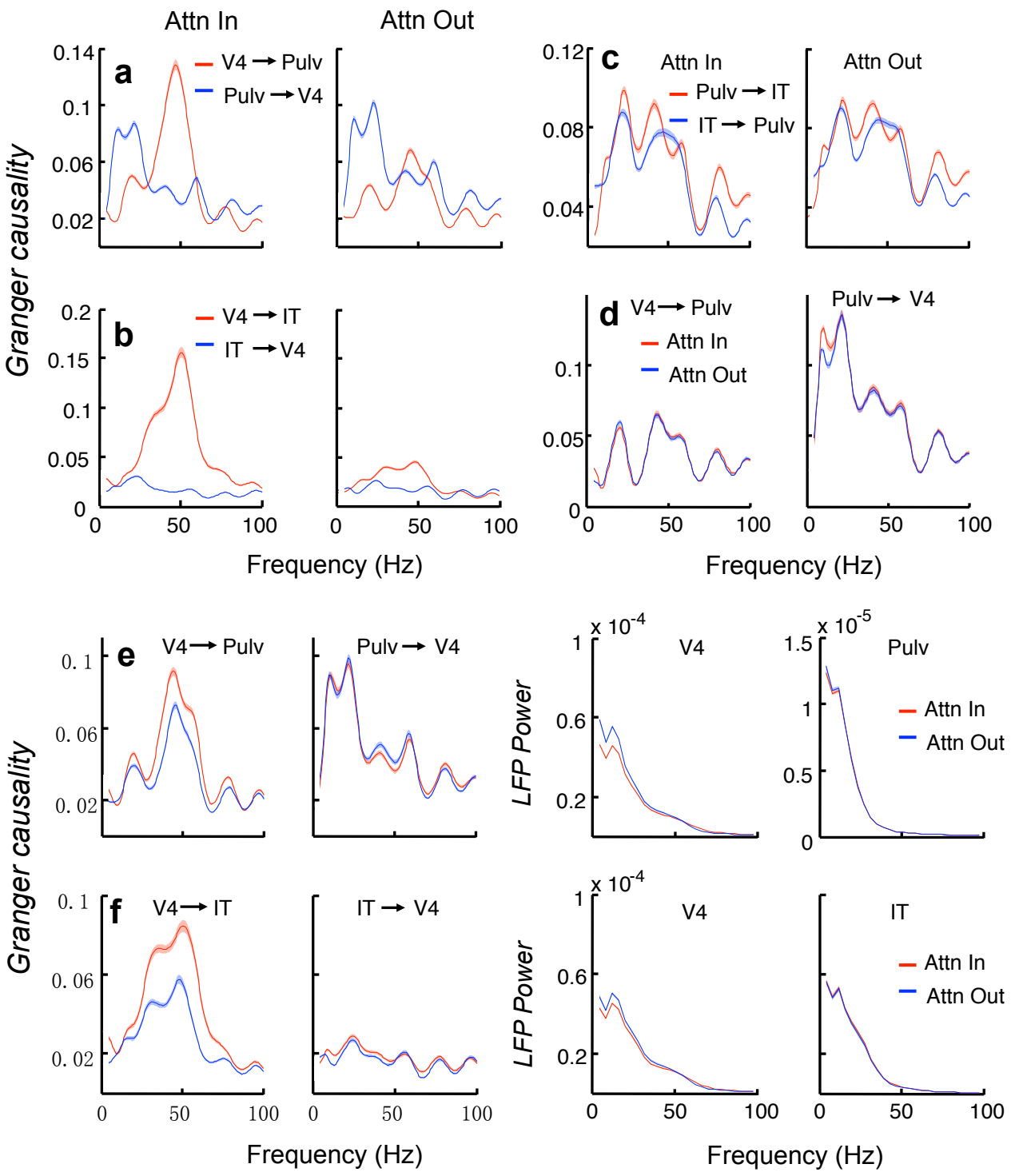
Attn In
Attn Out
a
V4 → Pulv
Pulv → V4
b
V4 → IT
IT → V4
c
Attn In
Pulv → IT
IT → Pulv
Attn Out
d
V4 → Pulv
Attn In
Attn Out
Pulv → V4
Granger causality
Frequency (Hz)
e
V4 → Pulv
Pulv → V4
f
V4 → IT
IT → V4
LFP Power
x 10^-4
V4
x 10^-5
Pulv
Attn In
Attn Out
IT

Figure S5

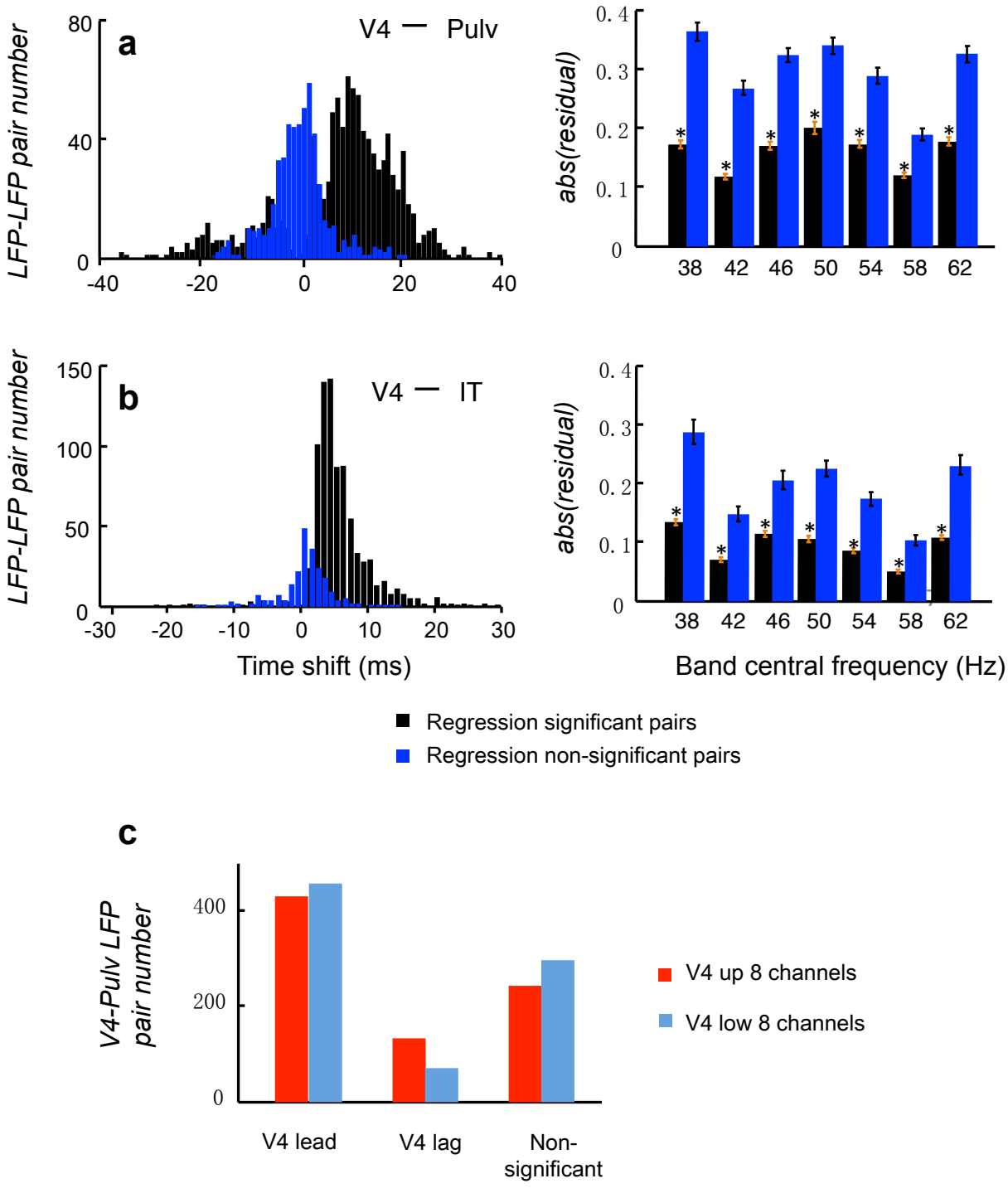
a
V4 — Pulv
LFP-LFP pair number
80
40
0
-40
-20
0
20
40
abs(residual)
0.4
0.3
0.2
0.1
0
38
42
46
50
54
58
62
b
V4 — IT
LFP-LFP pair number
150
100
50
0
-30
-20
-10
0
10
20
30
Time shift (ms)
abs(residual)
Band central frequency (Hz)
Regression significant pairs
Regression non-significant pairs
c
V4-Pulv LFP pair number
400
200
0
V4 lead
V4 lag
Non-significant
V4 up 8 channels
V4 low 8 channels

Figure S6

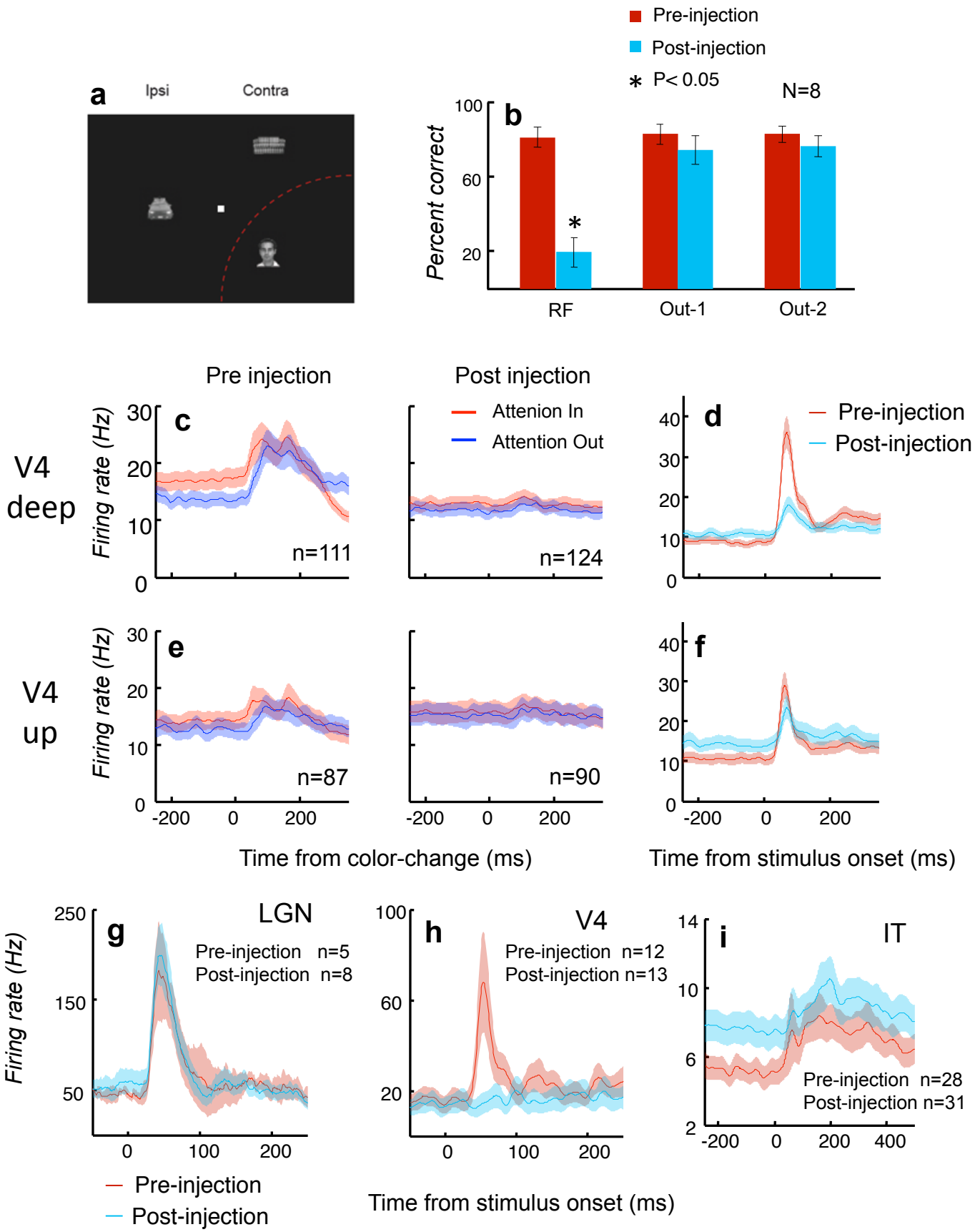
a
Ipsi
Contra
b
Pre-injection
Post-injection
* P< 0.05
N=8
Percent correct
100
60
20
*
RF
Out-1
Out-2
Pre injection
Post injection
V4 deep
c
Firing rate (Hz)
30
20
10
0
n=111
Attenion In
Attention Out
n=124
d
Pre-injection
Post-injection
40
30
20
10
0
V4 up
e
n=87
n=90
f
-200
0
200
Time from color-change (ms)
Time from stimulus onset (ms)
g
LGN
Pre-injection n=5
Post-injection n=8
250
150
50
h
V4
Pre-injection n=12
Post-injection n=13
100
60
20
i
IT
14
10
6
2
Pre-injection n=28
Post-injection n=31
400
Pre-injection
Post-injection
Time from stimulus onset (ms)

Figure S7

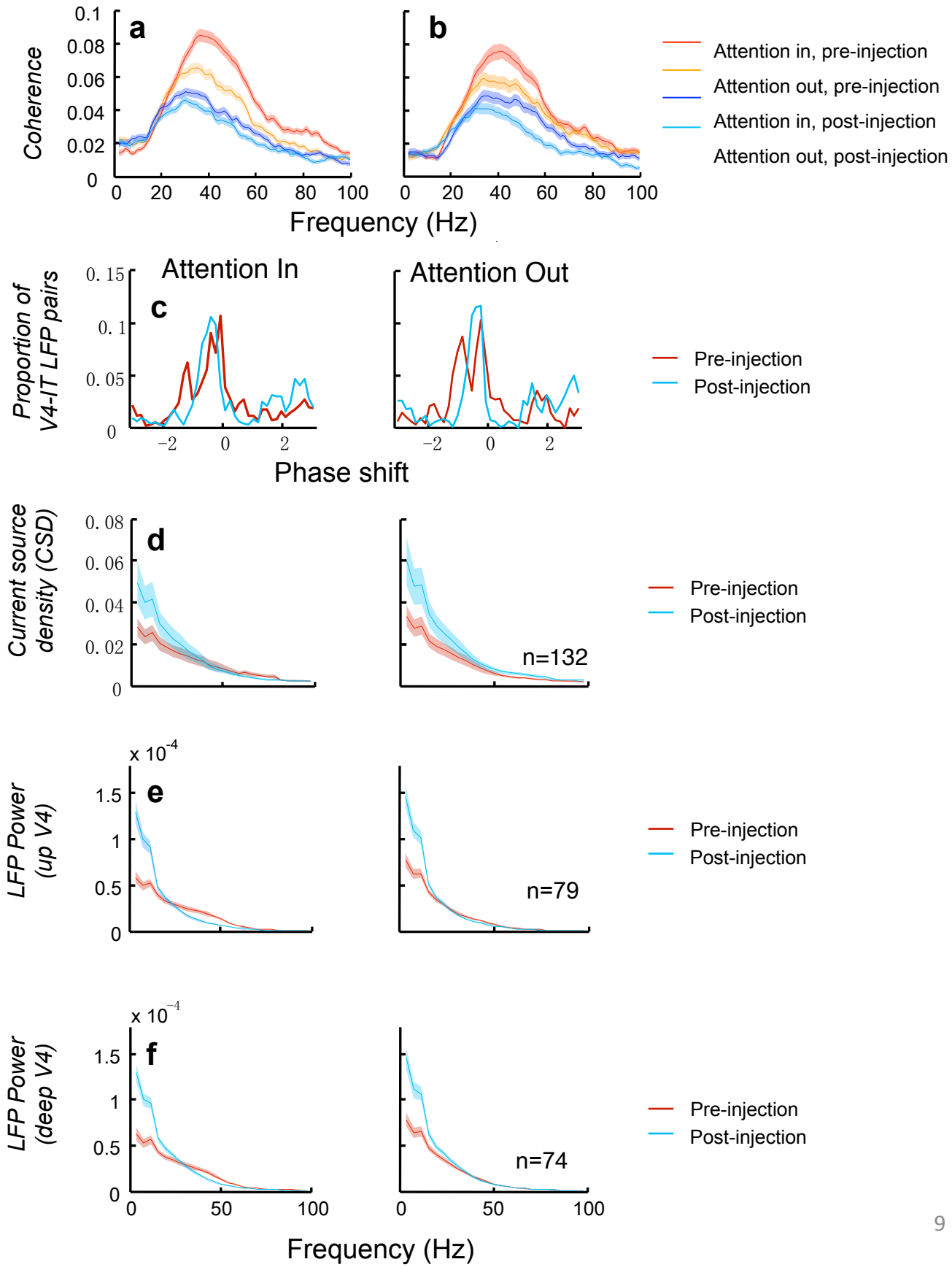
a
b
Coherence
0.1
0.08
0.06
0.04
0.02
0
0 20 40 60 80 100
Frequency (Hz)
Attention in, pre-injection
Attention out, pre-injection
Attention in, post-injection
Attention out, post-injection
Attention In
Attention Out
c
Proportion of V4-IT LFP pairs
0.15
0.1
0.05
0
−2 0 2
Phase shift
Pre-injection
Post-injection
d
Current source density (CSD)
0.08
0.06
0.04
0.02
0
n=132
Pre-injection
Post-injection
e
x 10^-4
LFP Power (up V4)
1.5
1
0.5
0
n=79
Pre-injection
Post-injection
f
x 10^-4
LFP Power (deep V4)
1.5
1
0.5
0
0 50 100
n=74
Pre-injection
Post-injection
Frequency (Hz)

Figure S8

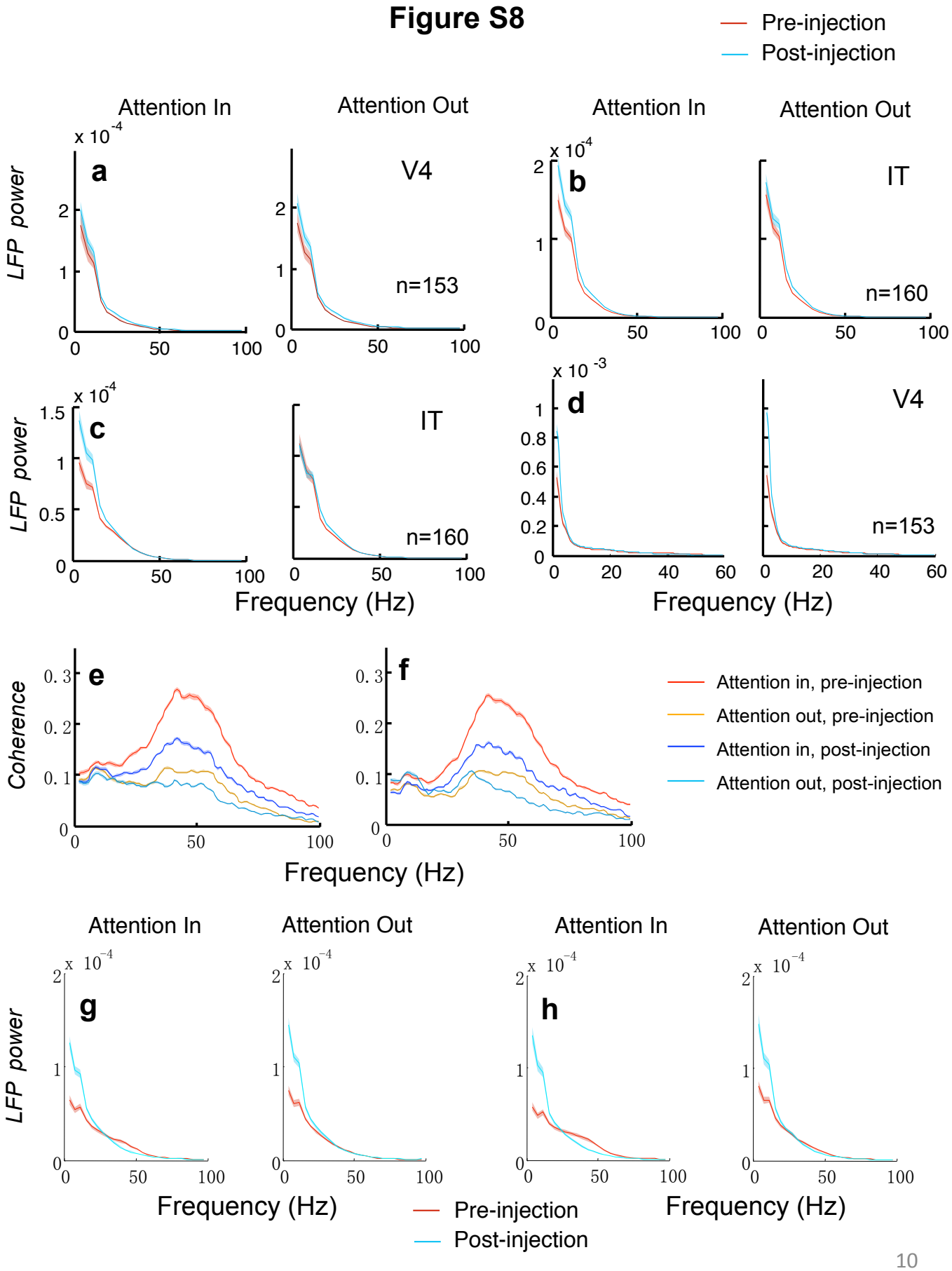
Pre-injection
Post-injection
Attention In
Attention Out
Attention In
Attention Out
a
V4
n=153
b
IT
n=160
c
IT
n=160
d
V4
n=153
LFP power
LFP power
Frequency (Hz)
Frequency (Hz)
e
f
Coherence
Attention in, pre-injection
Attention out, pre-injection
Attention in, post-injection
Attention out, post-injection
Frequency (Hz)
Attention In
Attention Out
Attention In
Attention Out
g
h
LFP power
Frequency (Hz)
Frequency (Hz)
Pre-injection
Post-injection

Supplementary Experimental Procedures

Data Analysis

To isolate the effects of spatial attention, we sorted trials into 2 groups: 'Attention In' and 'Attention Out'. On Attention In trials, the target was the stimulus inside the RF of the recorded neurons. On Attention Out trials, the target was outside the RF, and the RF stimulus was a distracter.

Spike density functions were calculated by convolving spike times with a Gaussian filter (σ =10 ms). For recording-only sessions, recording sites that showed a significant visual response (Wilcoxon rank-sum test, $p < 0.05$) were included for analysis. The interval used for statistical comparisons of firing rates was 50-250 ms after stimulus onset for the post-stimulus period and the last 200ms period prior to object stimulus onset for the pre-stimulus period. Object selectivity was defined on the basis of a significant ANOVA ($P < 0.05$) conducted on the responses (50-250ms after stimulus onset) to all stimuli at a site's best response location. The same standard was applied to sites in all three areas. Similar methods were used to determine a site's spatial selectivity based on its responses to stimuli at all three locations. If a site showed no spatial selectivity, it was excluded from analysis related to spatial attention. In the recording combined with pulvinar deactivation sessions, it was difficult to be sure that the same neurons were recorded before and after the deactivation. Therefore, all spiking sites before and after the injections were included in our analysis.

LFP signals were pre-processed for removal of the powerline artifact , and LFP phase shifts through the headstage and preamplifier were corrected using the utility program provided by Plexon Inc (FPAlign).

For recording-only sessions, only the data on correct trials were included for analysis. In the sessions with pulvinar deactivation, monkeys responded correctly to the target color-change in the affected area on only a small portion of trials. Therefore, to have enough data to analyze, we included both correct and error trials as long as monkeys maintained fixation through the time of the first target or distracter color-change for both the pre-deactivation and post-deactivation data.

Firing rate analysis. Averaged firing rates in Attention In and Out conditions were calculated by first subtracting average activity in the baseline period (the last 200 ms period before the stimulus onset) and then normalizing to the maximum rate in the Attention In condition for each site. The latencies of attentional modulation at the population level were determined from the distribution of averages of normalized responses across sites. We used a sliding window method to decide when the effects of attention first became significant in the population, starting from the time of stimulus onset in the cue-first trials. If a significant difference (Wilcoxon signed rank test, $P < 0.05$) was found in three successive and non-overlapping 10 ms windows between the Attention In and Attention Out responses, the time at the start of the first

window was defined as the latency of attention modulation. To test whether attention effect latencies from V4 and pulvinar populations were significantly different, we ran a two-sided permutation test with 5000 repeats as described in our previous study. For the calculation of attention latency for each recording site, we used the same sliding window method applied to the responses across trials. To quantify the magnitude of attentional modulation, the firing rates during the last 250 ms window preceding the earliest target or distracter color-change were averaged. The attention contrast index was then defined as ((Attention In -Attention Out) /(Attention In + Attention Out)) based on the averaged firing rates calculated for each site.

LFP power, Spike-LFP coherence and LFP-LFP coherence analysis. We used a multi-taper method for all these analysis, which was mainly performed in the Chronux MATLAB toolbox(www.chronux.org). For coherence, we used different tapers for the analysis of low and high frequencies. We used a single Hanning taper for low frequencies (4 - 25 Hz) and multitaper methods for higher frequencies (Fries et al., 2008) Coherency for two signals x and y is calculated as:

$$Cxy(f) = \frac{Sxy(f)}{\sqrt{Sx(f)Sy(f)}} \quad (1)$$

where *Sx(f)* and *Sy(f)* represent the auto-spectra and *Sxy(f)* the cross-spectrum of the two signals x and y. Auto-spectra and cross-spectra are averaged across trials before the coherence calculation. Data in the last 256 ms period prior to the earliest color-change at target or distracter location were included in the coherence analysis. The same number of trials for each condition (Attention In or Attention Out) was used for the calculation of coherence for a given pair of recording sites, to eliminate any bias from different sample sizes. All coherence calculations used the signals from two different electrodes, to preclude the possibility that spikes would actually contribute to the LFP recorded on the same electrode. To exclude the influence from factors such as different sustained firing rates, we shuffled the two signals across trials within each condition. Coherence of the two signals was corrected by subtracting the coherence computed from the shuffled data. Coherence at gamma frequencies (40-60Hz) was averaged and compared between Attention In and Attention Out conditions. To quantify the attentional effect, we calculated an attention modulation index ((Attention In -Attention Out) /(abs(Attention In) + abs(Attention Out))) based on the averaged gamma coherence, where 'abs' means the absolute value.

Granger causality analysis. We used an open source MATLAB toolbox – 'Granger causal connectivity analysis' (GCCA) . Frequency-domain Granger causalities were calculated in the same 256ms period as in coherence analysis between LFPs in V4, pulvinar and IT. Two preprocessing steps ('detrending' and 'demeaning')were applied to the LFPs. The best-fitting line of LFPs on each trial and ensemble mean of LFPs were subtracted using two functions cca_detrend() and cca_rm_ensemblemean() from the GCCA toolbox. We used a KPSS test to test the stationarity of LFP data after the preprocessing, and non-stationary LFP data were excluded in this analysis. Frequency-domain Granger causality

was calculated based on the stationary LFP data after preprocessing using a function cca_pwcausal() from the toolbox. Frequency-domain Granger causality is calculated as:

$$G_{j\to i}(f) = -\ln\left(1 - \frac{\left(\Sigma_{jj} - \left(\frac{\Sigma_{ij}^2}{\Sigma_{ii}}\right)\right)|H_{ij}(f)|^2}{S_{ii}(f)}\right) \quad (2)$$

where *Sii(f)* is the power spectrum of variable i at frequency f, H is the transfer matrix, and Σ is the noise covariance matrix (Seth, 2010). To investigate the effect of attention on interaction between these areas, the causalities at gamma frequencies (40-60Hz) were averaged and compared between Attention In and Attention Out conditions.

LFP gamma phase shift analysis. We also measured the directionality of V4 - pulvinar and V4 - IT interactions using the distribution of LFP phase lags between these areas (Schoffelen et al., 2005). To do so, we band-pass filtered LFP signals to generate 7 frequency bands (36-40, 40-44, 44-48, 48-52, 52-56, 56-60, 60-64Hz) around 50Hz using a two-way least squares FIR filter, which covered the frequencies of maximum gamma coherence between these areas. A Hilbert transformation was applied to these bands to calculate their instantaneous phases. The instantaneous phase lags of these bands between two areas were calculated by subtracting the phase values of one area, which generated 7 phase shift distributions for the 7 gamma bands. The mean phase shift at each band was estimated by calculating the circular mean of its phase shift distribution. We analyzed the relationship between central frequencies and mean phase shifts of the 7 gamma bands using a linear regression method. Only LFP pairs showing that mean phase shifts significantly increased or decreased linearly with the frequency were used to estimate the time lag between gamma oscillations in two areas. The time lag was estimated as S/(2*π), where S was the slope of the phase shift changing along the frequency. We performed this analysis on LFPs in the same 256 ms period as used in the coherence analysis, and estimated the time lags on Attention In and Attention Out trials, respectively.

References

Fries P, Womelsdorf T, Oostenveld R, Desimone R (2008) The effects of visual stimulation and selective visual attention on rhythmic neuronal synchronization in macaque area V4. J Neurosci 28:4823-4835.

Schoffelen JM, Oostenveld R, Fries P (2005) Neuronal coherence as a mechanism of effective corticospinal interaction. Science 308:111-113.

Seth AK (2010) A MATLAB toolbox for Granger causal connectivity analysis. J Neurosci Methods 186:262-273.